Electronic Supplementary Information
Flow-enhanced spatiotemporal pH oscillations

Fatima Shoeb and István Szalai
Institute of Chemistry, Eötvös Loránd University, Budapest, Hungary

istvan.szalai@ttk.elte.hu

1 Supplementary methods

1.1 Derivation of the numerical models

Numerical simulations of the pH oscillators were performed using the extended Rábai model.[1]

$$\mathrm{A^- + H^+ \rightleftharpoons HA} \tag{R1}$$
$$\mathrm{HA + B \xrightarrow{H^+} H^+ + P_1} \tag{R2}$$
$$\mathrm{B + H^+ + C \longrightarrow P_2} \tag{R3}$$
$$\mathrm{B + H^+ + HA \longrightarrow P_3} \tag{R4}$$
$$\mathrm{H^+ + OH^- \rightleftharpoons H_2O} \tag{R5}$$

The corresponding rate equations are as follows:

$$v_1 = k_1[\mathrm{A^-}][\mathrm{H^+}] - k_{-1}[\mathrm{HA}] \tag{1}$$
$$v_2 = (k_2[\mathrm{H^+}] + k_2')[\mathrm{HA}][\mathrm{B}] \tag{2}$$
$$v_3 = k_3[\mathrm{B}][\mathrm{C}][\mathrm{H^+}] \tag{3}$$
$$v_4 = k_4[\mathrm{B}][\mathrm{HA}][\mathrm{H^+}] \tag{4}$$
$$v_5 = k_5[\mathrm{H^+}][\mathrm{OH^-}] - k_{-5} \tag{5}$$

The dynamics of the CSTR content is governed by the following set of equations:

$$d[\mathrm{H^+}]/dt = -v_1 + v_2 - v_3 - v_5 + \frac{1}{\tau}([\mathrm{H^+}]_0 - [\mathrm{H^+}]) \tag{6}$$

$$d[\mathrm{A^-}]/dt = -v_1 + \frac{1}{\tau}([\mathrm{A^-}]_0 - [\mathrm{A^-}]) \tag{7}$$

$$d[\mathrm{HA}]/dt = v_1 - v_2 - v_4 + \frac{1}{\tau}([\mathrm{HA}]_0 - [\mathrm{HA}]) \tag{8}$$

$$d[\mathrm{B}]/dt = -v_2 - v_3 - v_4 + \frac{1}{\tau}([\mathrm{B}]_0 - [\mathrm{B}]) \tag{9}$$

$$d[\mathrm{C}]/dt = -v_3 + \frac{1}{\tau}([\mathrm{C}]_0 - [\mathrm{C}]) \tag{10}$$

$$d[\mathrm{OH^-}]/dt = -v_5 + \frac{1}{\tau}([\mathrm{OH^-}]_0 - [\mathrm{OH^-}]) \tag{11}$$

$$\tag{12}$$

The parameters are: $k_1 = 10^{10}\,\mathrm{M^{-1}s^{-1}}$, $k_{-1} = 10^3\,\mathrm{s^{-1}}$, $k_2 = 10^7\,\mathrm{M^{-2}s^{-1}}$, $k_{2'} = 10\,\mathrm{M^{-1}s^{-1}}$, $k_3 = 10^5\,\mathrm{M^{-1}s^{-1}}$, $k_4 = 2\times10^5\,\mathrm{M^{-1}s^{-1}}$, $k_5 = 1.4\times10^{11}\,\mathrm{M^{-1}s^{-1}}$, $k_{-5} = 1.4\times10^3\,\mathrm{M\,s^{-1}}$, $\tau = 300\,\mathrm{s}$.

For the one-dimensional reaction–diffusion–advection model, the governing equations are

$$\partial_t[\mathrm{H^+}] = -v_1 + v_2 - v_3 - v_5 - u\partial_x[\mathrm{H^+}] + D\partial_x^2[\mathrm{H^+}] \tag{13}$$

$$\partial_t[\mathrm{A^-}] = -v_1 - u\partial_x[\mathrm{A^-}] + D\partial_x^2[\mathrm{A^-}] \tag{14}$$

$$\partial_t[\mathrm{HA}] = v_1 - v_2 - v_4 - u\partial_x[\mathrm{HA}] + D\partial_x^2[\mathrm{HA}] \tag{15}$$

$$\partial_t[\mathrm{B}] = -v_2 - v_3 - v_4 - u\partial_x[\mathrm{B}] + D\partial_x^2[\mathrm{B}] \tag{16}$$

$$\partial_t[\mathrm{C}] = -v_3 - u\partial_x[\mathrm{C}] + D\partial_x^2[\mathrm{C}] \tag{17}$$

$$\partial_t[\mathrm{OH^-}] = -v_5 - u\partial_x[\mathrm{OH^-}] + D\partial_x^2[\mathrm{OH^-}] \tag{18}$$

$$\tag{19}$$

1.2 Diffusion coefficients and model assumptions

In most numerical simulations, equal diffusion coefficients were assumed for all chemical species ($D = 10^{-5}\,\mathrm{cm^2\,s^{-1}}$). This approximation was adopted to isolate the role of nonlinear kinetics and advection in shaping the observed spatiotemporal dynamics. To examine the potential influence of differential diffusion, particularly long-range proton-mediated activation, additional simulations were performed with $D_{\mathrm{H^+}} > D_{\mathrm{other}}$.

Dirichlet boundary conditions were imposed at the inlet, $x = 0$, for all feed species; for example, $[\mathrm{H^+}](x=0) = [\mathrm{H^+}]_0$. No-flux boundary conditions were imposed at the downstream end, $x = L_x$; for example, $(\partial_x[\mathrm{H^+}])_{x=L_x} = 0$. The partial differential equations were discretized with a standard second-order finite-difference scheme on an equidistant grid of 300–600 points. The resulting set of ordinary differential equations was solved with the CVODE solver from the SUNDIALS package[2] using the backward differentiation formula method. The absolute and relative error tolerances were 10^{-14} and 10^{-7}, respectively.

1.3 Relation between one-dimensional simulations and experiments

The numerical model considers one-dimensional reaction–diffusion–advection dynamics along the axial direction of the flow channel. This approach captures the dominant transport processes governing residence time, front propagation, and oscillation nucleation. In the experiments, the flow is laminar

and characterized by a parabolic velocity profile, which may give rise to cross-sectional gradients and cusp-shaped reaction fronts.

The one-dimensional model therefore provides an effective axial description that neglects radial variations while preserving the essential timescale competition among reaction, diffusion, and advection. The qualitative agreement between experiments and simulations indicates that the observed oscillatory regime is primarily controlled by axial transport and nonlinear kinetics. Extensions to higher-dimensional models would enable explicit treatment of radial velocity gradients and differential-diffusion effects.

1.4 Characteristic timescales and Damköhler numbers

To rationalize the role of flow in the reaction–diffusion–advection dynamics, it is useful to compare the advective residence time with intrinsic kinetic timescales of the activating and inhibitory pathways. The advective timescale is defined as

$$\tau_{\mathrm{adv}} = \frac{L(x)}{u},$$

where $L(x)$ is the characteristic axial distance over which the dynamics are evaluated and u is the mean flow velocity.

The autocatalytic proton-producing pathway provides rapid local activation, characterized by a timescale τ_{act} that can be estimated from the rising edge of the pH transition in batch or CSTR simulations. Inhibitory pathways introduce delayed negative feedback and are characterized by fast and slow inhibitory timescales, $\tau_{\mathrm{inh,fast}}$ and $\tau_{\mathrm{inh,slow}}$, which correspond to the recovery dynamics following the acidic transition.

Based on these timescales, pathway-specific Damköhler numbers can be defined as

$$Da_{\mathrm{act}} = \frac{\tau_{\mathrm{adv}}}{\tau_{\mathrm{act}}}, \quad Da_{\mathrm{inh,fast}} = \frac{\tau_{\mathrm{adv}}}{\tau_{\mathrm{inh,fast}}}, \quad Da_{\mathrm{inh,slow}} = \frac{\tau_{\mathrm{adv}}}{\tau_{\mathrm{inh,slow}}}.$$

1.5 Supplementary figures

1.5.1 Experiments

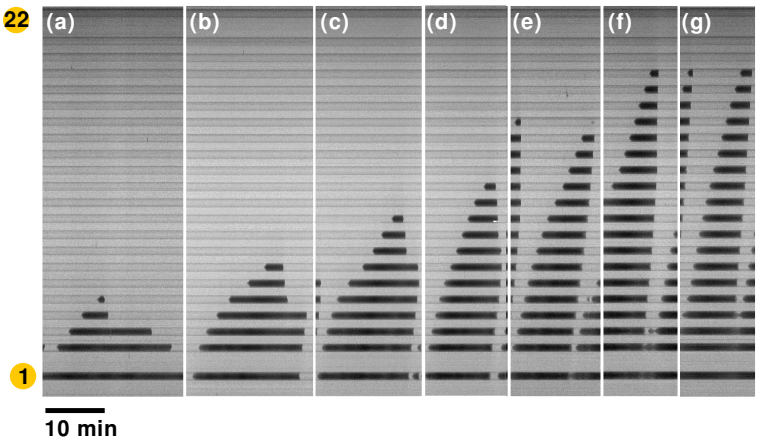

Figure S1 Time-space plot of spatiotemporal oscillations in the bromate-sulfite reaction at different flow rates: a) $v =$ 0.06 mL/min, b) $v = 0.08$ mL/min, c) $v = 0.10$ mL/min, d) $v = 0.12$ mL/min, e) $v = 0.14$ mL/min, f) $v = 0.16$ mL/min, g) $v = 0.18$ mL/min. The color indicates the pH of the mixture in the flow channel: dark indicates high pH (above 5.4), and light indicates low pH (below 3.8). Experimental conditions: t =25 °C, $[BrO_3^-]_{A0}$=660 mM, $[SO_3^{2-}]_{B0}$=60 mM, $[H_2SO_4]_{A0}$=5 mM, $[BCG]_0$=0.1 mM.

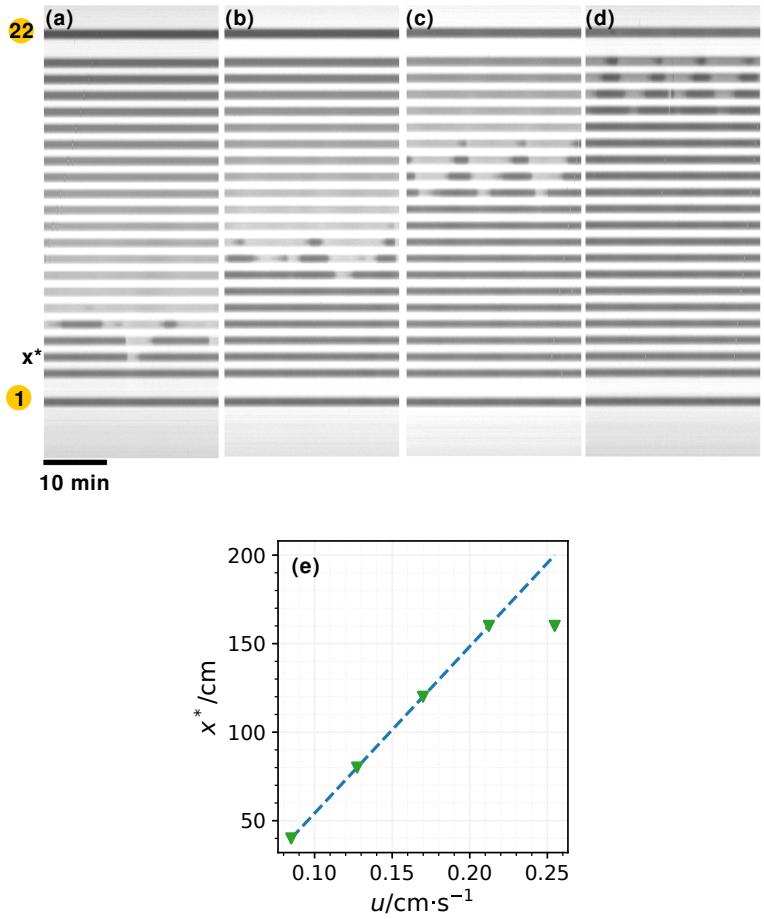

Figure S2 Time-space plot of spatiotemporal oscillations in the bromate-sulfite-ferrocyanide reaction at different flow rates: a) $v = 0.04$ mL/min, b) $v = 0.06$ mL/min, c) $v = 0.08$ mL/min, d) $v = 0.10$ mL/min. The color indicates the pH of the mixture in the flow channel: dark indicates high pH (above 5.4), and light indicates low pH (below 3.8). The dependence of the position of the nucleation point on u is shown in the bottom panel. Experimental conditions: t =35 °C, $[BrO_3^-]_{A0}$=130 mM, $[SO_3^{2-}]_{B0}$=80 mM, $[Fe(CN)_6^{4-}]_{B0}$=40 mM, $[H_2SO_4]_{A0}$=7 mM, $[BCG]_0$=0.1 mM.

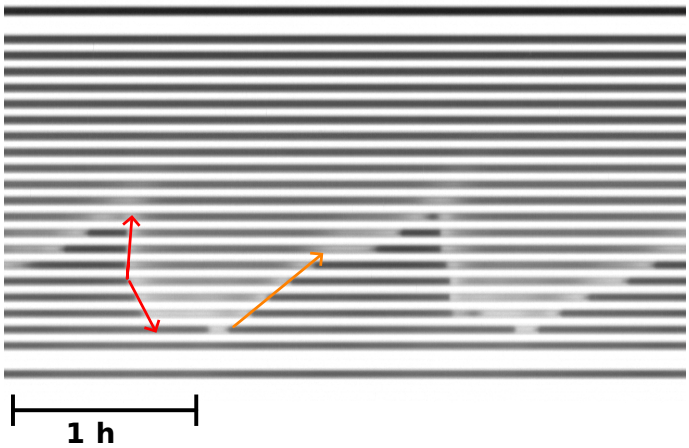

Figure S3 Time-space plot of spatiotemporal oscillations in the bromate-sulfite-ferrocyanide reaction at $t = 25\,^{\circ}\mathrm{C}$. The color indicates the pH of the mixture in the flow channel: dark indicates high pH (above 5.4), and light indicates low pH (below 3.8). Experimental conditions: $v = 0.14$ mL/min ($u = 0.30$ cm/s), $[BrO_3^-]_{A0}$=130 mM, $[SO_3^{2-}]_{B0}$=80 mM, $[Fe(CN)_6^{4-}]_{B0}$=40 mM, $[H_2SO_4]_{A0}$=7 mM, $[BCG]_0$=0.1 mM.

1.5.2 Simulations

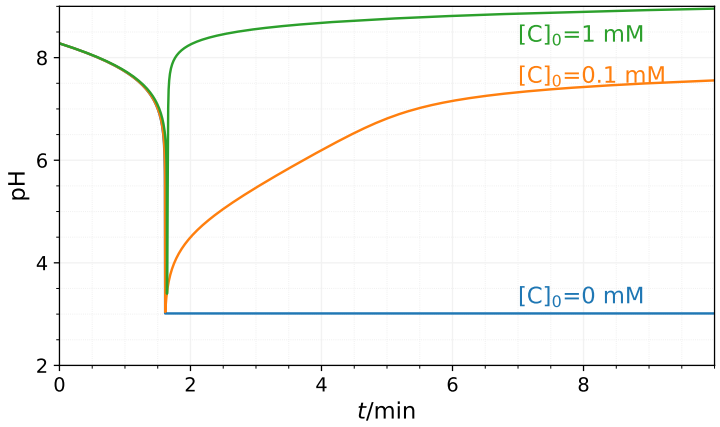

Figure S4 Simulated batch dynamics of the Rábai model in the absence of C (blue) and in the presence of C at $[C]_0$=0.1 mM and $[C]_0$=1 mM. The initial conditions are $[A^-]_0$=10 mM, $[B]_0$=12 mM, and $[H^+]_0$=1 mM.

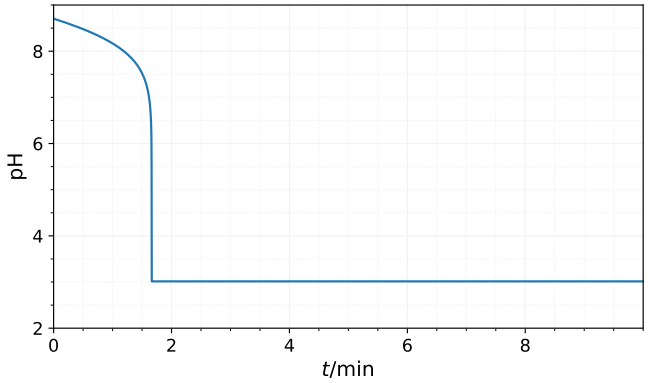

Figure S5 Simulated batch dynamics of the Rábai model in the absence of C at a high $[B]_0/[A^-]_0$ ratio. The initial conditions are $[A^-]_0$=52 mM, $[B]_0$=80 mM, $[H^+]_0$=1 mM, and $[C]_0$=0 mM.

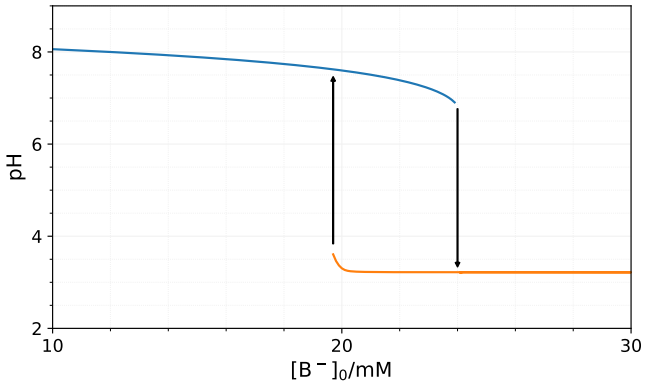

Figure S6 Simulated bistability in the Rábai model under CSTR conditions in the absence of C. The initial conditions are $[A^-]_0$=10 mM, $[B]_0$=12 mM, $[H^+]_0$=1 mM, $[C]_0$=0 mM, and $\tau = 300$ s.

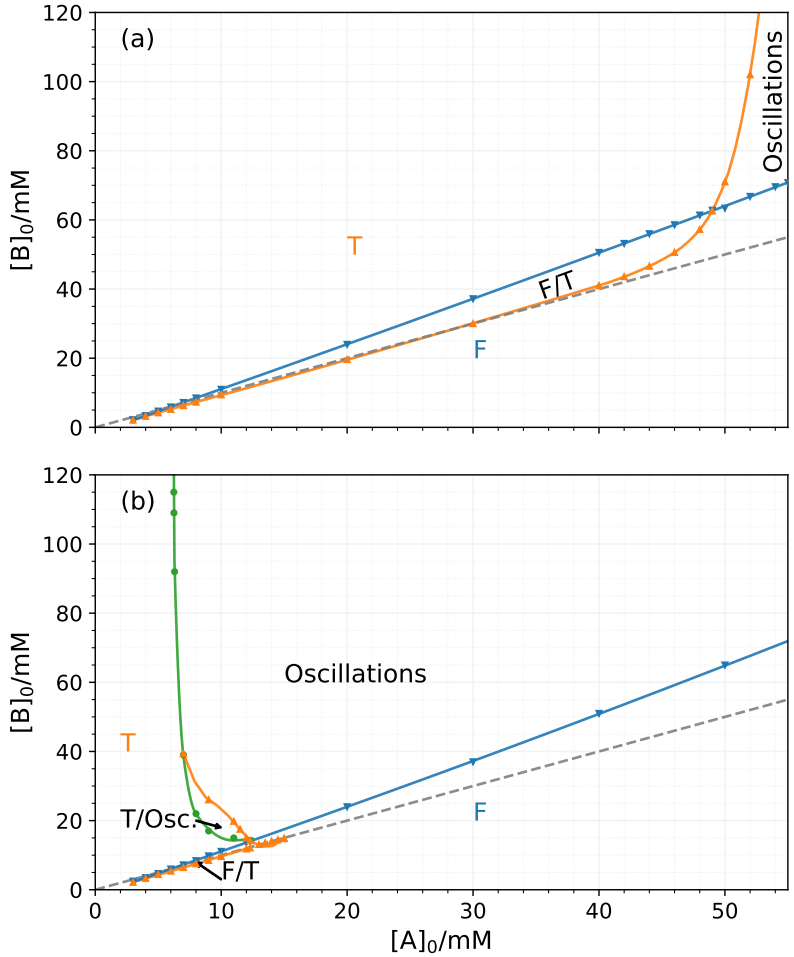

Figure S7 Simulated nonequilibrium phase diagrams in the absence of C (a) and in the presence of C at $[C]_0$=1 mM (b). The solid lines are spline curves fitted to the numerically computed points (triangles). The blue, orange, and green colors correspond to the stability limits of the F, T, and oscillatory states, respectively. The dashed gray lines indicate the $[B]_0/[A^-]_0$=1 ratio.

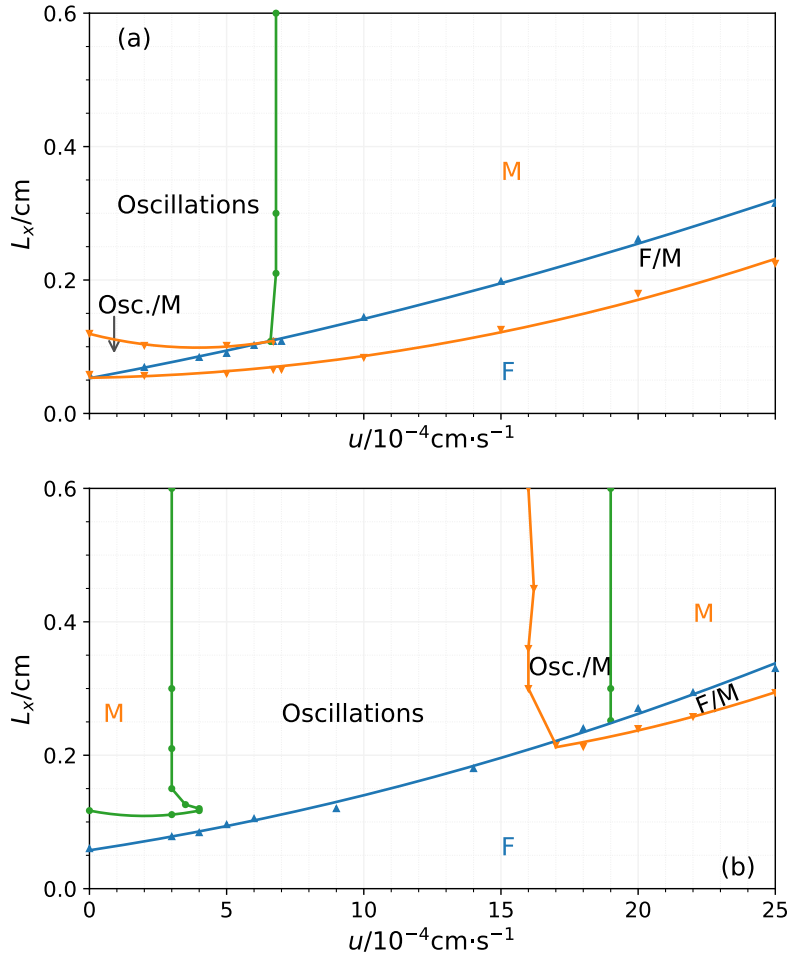

Figure S8 Simulated nonequilibrium phase diagrams in the presence of C at $[C]_0$=2 mM (a) and $[C]_0$=10 mM (b). The orange and blue triangles indicate the stability limits of the F and M states, respectively. The parameters used in the simulations are $[B]_0$=12 mM and $[A^-]_0$=10 mM. The solid lines are spline curves fitted to the numerically computed points (triangles).

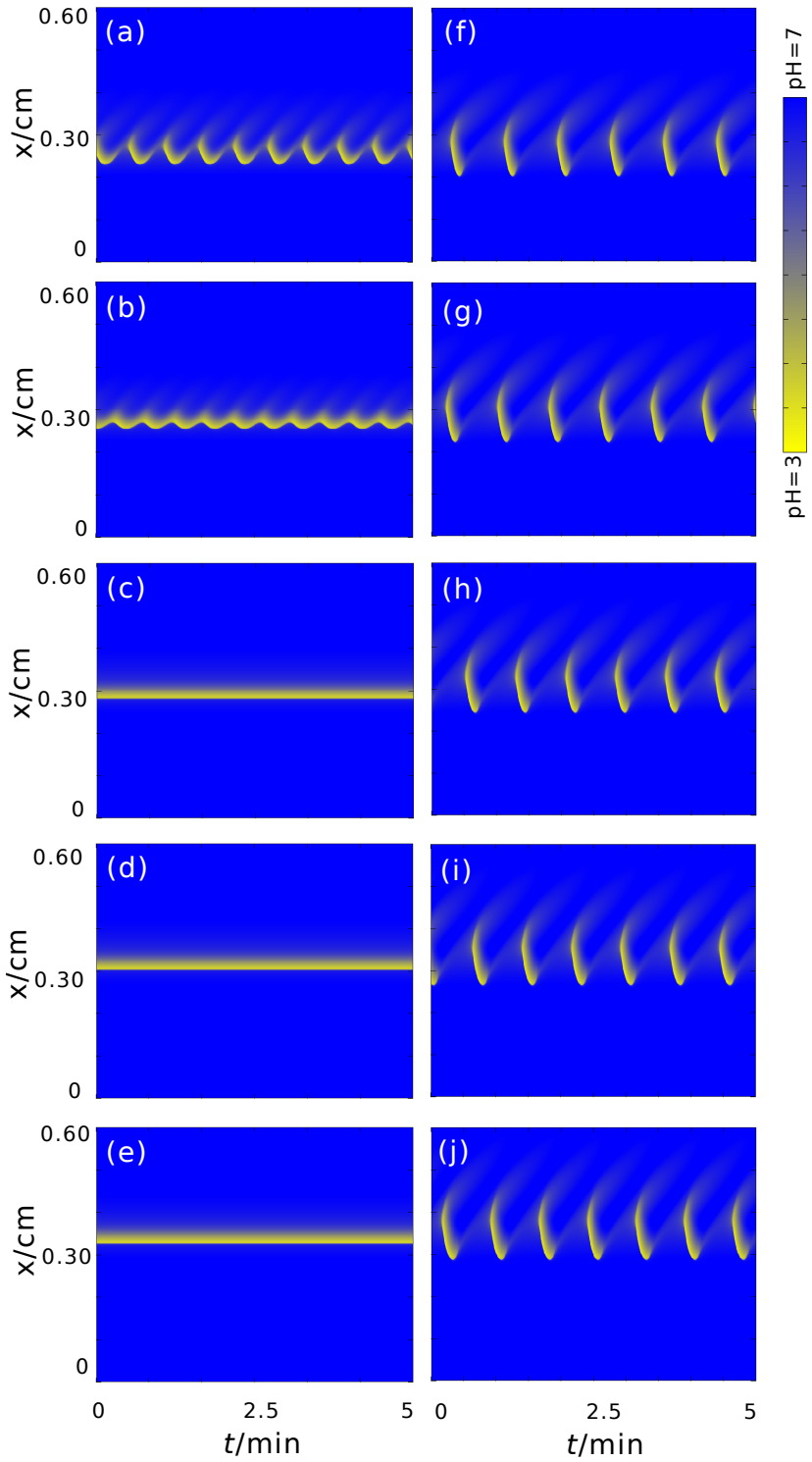

Figure S9 Simulated time-space plots at $D_{H^+} = D_{other}$ (a–e) and $D_{H^+} = 4D_{other}$ (f–j). The parameters used in the simulations are $u_0 = 1.8 \times 10^{-3}$ cm/s (a and f), $u_0 = 2.0 \times 10^{-3}$ cm/s (b and g), $u_0 = 2.2 \times 10^{-3}$ cm/s (c and h), $u_0 = 2.4 \times 10^{-3}$ cm/s (d and i), $u_0 = 2.6 \times 10^{-3}$ cm/s (e and j), $[B]_0$=12 mM, $[A^-]_0$=9 mM, $[HA]_0$=1 mM, $[C]_0$=10 mM, $[H^+]_0$=10^{-7} M, and L_x=0.6 cm.

Notes and references

[1] G. Rabai, *ACH - Models Chem.*, 1998, **135**, 381–392.

[2] A. C. Hindmarsh, P. N. Brown, K. E. Grant, S. L. Lee, R. Serban, D. E. Shumaker and C. S. Woodward, *ACM Transactions on Mathematical Software (TOMS)*, 2005, **31**, 363–396.